Optical Materials 90 (2019) 200–207

Contents lists available at ScienceDirect

Optical Materials

journal homepage: www.elsevier.com/locate/optmat

# $Yb^{3+}/Er^{3+}$ codoped $GeO_2$–PbO–$PbF_2$ glass ceramics for ratiometric upconversion temperature sensing based on thermally and non-thermally coupled levels

A.A. Kalinichev[a], M.A. Kurochkin[a], A.Y. Kolomytsev[a], R.S. Khasbieva[b], E. Yu Kolesnikov[c], E. Lähderanta[d], I.E. Kolesnikov[a,d,*]

[a] St. Petersburg State University, 7/9 Universitetskaya nab., 199034, St. Petersburg, Russia
[b] Bashkir State Medical University, Teatralnaya Street 2a, 450000, Ufa, Russia
[c] Volga State University of Technology, Lenin sqr. 3, 424000, Yoshkar-Ola, Russia
[d] Lappeenranta University of Technology LUT, Skinnarilankatu 34, 53850, Lappeenranta, Finland

ARTICLE INFO

*Keywords:*
$Er^{3+}$
Upconversion
Sensors
Optical thermometry
Sensitivity

ABSTRACT

The contactless real-time temperature sensing technique with high temporal and spatial resolution is in high demand for the countless applications. Here, the $Yb^{3+}/Er^{3+}$ codoped $GeO_2$–PbO–$PbF_2$ glass ceramics synthesized via the melt-quenching technique has been presented as an optical thermometer. The thermal sensing was designed based on the temperature dependent fluorescence intensity ratios of thermally ($^2H_{11/2}$ and $^4S_{3/2}$) and non-thermally ($^2H_{11/2}$ and $^4F_{9/2}$) coupled $Er^{3+}$ levels. The ratiometric techniques provide the thermal sensing within the temperature range of 300–466 K. The absolute and relative thermal sensitivities as well as the temperature resolution were calculated and compared with other $Yb^{3+}/Er^{3+}$-doped materials. The temperature of the microelectronic component on the printed circuit board was defined using the optical thermometry as a proof of concept revealing $Yb^{3+}/Er^{3+}$ codoped $GeO_2$–PbO–$PbF_2$ phosphor to be a promising candidate for precise non-contact thermal sensor.

## 1. Introduction

As a fundamental physical parameter, temperature plays a significant role in many biological and technical processes. Therefore, the real-time and in situ temperature sensing with the high temporal and spatial resolution is extremely desired to control and govern these processes. Due to the miniaturization of the electronic components and necessity of defining temperature in the harsh environment (high electromagnetic field, corrosive circumstances, etc.), the non-contact sensing techniques have attracted great attention last years [1–5]. As one of the non-contact temperature sensing strategies, a luminescence thermometry has gained considerable interest because of its advantages of fast response, noninvasive operation and high-spatial resolution [6]. Among the thermal sensing methods based on various temperature dependent luminescence parameters, the ratiometric approach is usually considered as the most perspective one. This technique involves the comparison of luminescence intensities between two energy levels, whose respective emission intensity is thermally modulated with the temperature [7,8]. The ratiometric luminescence thermometry is a self-calibrating technique, which provides accurate measurements without influences of the fluorescence losses, time exposure and pump power fluctuation [9–13].

The rare earth-doped upconverting materials have been intensively investigated, largely focusing on the potential applications such as nanoscale thermometry, diagnostics and therapy [14]. The rising interest in an upconverting nanoparticles is connected with their unique excitation schemes where they can be excited with near-infrared (NIR) light and emit higher energy photons spanning the ultraviolet, visible and NIR regions via a multiphoton excitation process, known as upconversion [15–17]. The upconverted luminescence has advantages when compared with the conventional fluorescence for several reasons. The NIR excitation light causes minimal photodamage, induces practically no autofluorescence background, and can penetrate biological tissue much deeper [18,19].

The host materials affect the performances of optical temperature sensors especially based on upconversion luminescence. It is well-known that hosts with lower phonon energies will demonstrate higher upconversion luminescence efficiency, which will increase the thermal

* Corresponding author. St. Petersburg State University, 7/9 Universitetskaya nab., 199034, St. Petersburg, Russia.
*E-mail addresses:* ie.kolesnikov@gmail.com, ilya.kolesnikov@spbu.ru (I.E. Kolesnikov).

https://doi.org/10.1016/j.optmat.2019.02.035
Received 5 November 2018; Received in revised form 13 February 2019; Accepted 17 February 2019

measurement accuracy [20]. Another important feature of the host matrix is mechanical and thermal stability, which makes them suitable for utilizing in harsh environments [21]. The oxyfluoride glass ceramics is a host material combining low cut-off phonon energy from fluorides and desirable mechanical and chemical characteristics from oxides [22,23]. Other advantages of oxyfluoride glass ceramics are: ability to stabilize metastable crystalline fluoride phases that cannot be prepared and/or preserved at room temperature; preventing of fluoride nanoparticle agglomeration by the glass phase; inactivation of the highly developed and active surface of the nanoparticles (it is important in case of fluoride nanoparticles which can be easily quenched by the adsorption of water on their surfaces) [24]. It was reported that the lead fluorogermanate glasses have advantages compared to the fluoride glass systems including high chemical stability, good thermal stability and excellent glass forming characteristics [25].

One of the most well-known examples of an optical thermometer exploiting the temperature sensitive emissions is the $Er^{3+}$ ion [26–28]. In particular, the temperature induced change in the fluorescence intensity ratio (FIR) between two green emission bands originating from the $^2H_{11/2}$ and $^4S_{3/2}$ excited states of $Er^{3+}$ can be used for thermal sensing. The $Yb^{3+}$ ion is usually doped as a sensitizer in the upconvertion process to enhance the pump efficiency of $Er^{3+}$ due to the large absorption cross section around 980 nm of $Yb^{3+}$ and efficient energy transfer from $Yb^{3+}$ to $Er^{3+}$ [29–31].

Here, $GeO_2$–PbO–$PbF_2$–$YbF_3$–$ErF_3$ glass ceramics fabricated through melt-quenching technique was demonstrated as a ratiometric luminescence temperature sensor based on the thermally and non-thermally coupled energy levels. All obtained results indicate that the studied $Yb^{3+}/Er^{3+}$-codoped sample could be considered as a potential candidate for the thermal sensing.

## 2. Experimental

A precursor glass sample with the molar composition of $50GeO_2$–$35PbO$–$5PbF_2$–$8.5YbF_3$–$1.5ErF_3$ was fabricated from the high-purity chemicals. The starting batches were thoroughly mixed, put in a platinum crucible and melted at 1000 °C for 15 min in normal air atmosphere. Then the melts were quenched on the preheated copper plate and annealed below $T_g$ (at 360 °C) in order to eliminate internal stresses. The glass samples were additionally annealed at 400 °C for 7 h to obtain the $PbF_2$ crystallization. All heat-treated samples were kept in the furnace to cool to the room temperature.

X-ray phase analysis was carried out with Rigaku « Miniflex II » diffractometer with $CuK_\alpha$-radiation (λ = 1.5406 Å). Electron micrograph images and elemental analysis were obtained using Zeiss Merlin electron microscope with Oxford Instruments INCAx-act accessory. Photoluminescence properties were studied with modular fluorescence spectrometer Fluorolog-3 upon 973 nm diode laser. This excitation source and T64000 Raman Spectrometer were used for thermal sensing experiments. The laser beam was focused onto the sample by using a 4x long working distance microscope objective (NA 0.1). The fluorescence was collected by using the same microscope objective and was spectrally analyzed by single spectrometer and a Peltier cooled Synapse CCD detector. The thermal experiments were carried out using heating stage controlled with ThorLabs TC200 with a resolution of 0.1 °C.

## 3. Results and discussion

The XRD pattern of $GeO_2$–PbO–$PbF_2$–$YbF_3$–$ErF_3$ glass-ceramics is shown in Fig. 1. As it can be seen, all the peaks in the diffraction pattern coincide with cubic phase of $PbF_2$ (space group Fm-3m, JCPDS 06-0251). No impurity phase was detected. The observed broad band about 24° can be attributed to the glass host.

The average size of coherent scattering region (crystallite size) can be calculated using the Scherer's approach [32]:

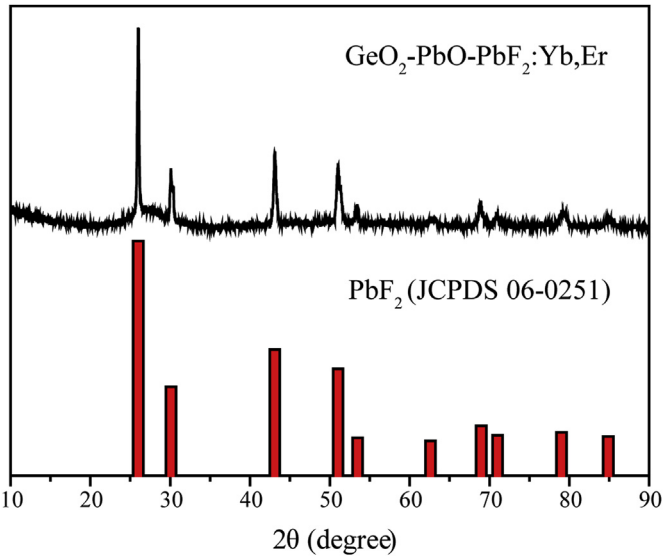


**Fig. 1.** a) XRD patterns of $GeO_2$–PbO–$PbF_2$–$YbF_3$–$ErF_3$ glass-ceramics powder with the standard card of $PbF_2$ (JCPDS 06-0251).

$$D = \frac{0.9\lambda}{cos\theta\sqrt{\beta^2 - \beta_0^2}} \quad (1)$$

where D is an average size of the ordered (crystalline) domains, which may be smaller or equal to the grain size; λ is the X-ray wavelength; β is the full width at half-maximum (FWHM) of a diffraction line located at θ in radians; θ is the Bragg angle; $\beta_0$ is the scan aperture of the diffractometer. Calculated average crystallite size (coherent-scattering region) was about 30 nm.

Fig. 2 shows the scanning electron microphotographs of the synthesized glass-ceramics powder with different magnifications. As seen from the micrographs, the powder consists of the agglomerated particles with size from 100 nm to 1 μm.

To study elemental analysis of the glass-ceramics powder, EDX technique was used (Fig. 3). The signals from germanium, oxide, lead, fluorine, erbium and ytterbium were observed, which confirms formation of $GeO_2$-PbO-$PbF_2$-$YbF_3$-$ErF_3$ sample.

The absorption spectrum of $GeO_2$–PbO–$PbF_2$–$YbF_3$–$ErF_3$ glass-ceramics powder was measured in the spectral region of 200–1200 nm (Fig. 4). It consists of the characteristic narrow lines attributed to the 4f intra-configurational electron transitions in the $Er^{3+}$ and $Yb^{3+}$ ions: 234 nm ($Er^{3+}$, $^4I_{15/2}$–$^4D_{3/2}$), 306 nm ($Er^{3+}$, $^4I_{15/2}$–$^2P_{3/2}$), 486 nm ($Er^{3+}$, $^4I_{15/2}$–$^4F_{7/2}$), 522 nm ($Er^{3+}$, $^4I_{15/2}$–$^2H_{11/2}$), 540 nm ($Er^{3+}$, $^4I_{15/2}$–$^4S_{3/2}$), 655 nm ($Er^{3+}$, $^4I_{15/2}$–$^4F_{9/2}$) and 974 nm ($Yb^{3+}$, $^2F_{7/2}$–$^2F_{5/2}$).

The excitation spectrum of $GeO_2$–PbO–$PbF_2$–$YbF_3$–$ErF_3$ glass-ceramics powder monitored at 655 nm ($^4F_{9/2}$–$^4I_{15/2}$) is presented in Fig. 5a. Similar to absorption spectrum, it consists of the narrow lines centered at 355, 363, 378 and 405 nm, which can be assigned to the $^4I_{15/2}$–$^4G_{7/2}$, $^4I_{15/2}$–$^4G_{9/2}$, $^4I_{15/2}$–$^4G_{11/2}$, and $^4I_{15/2}$–$^2H_{9/2}$ transitions of $Er^{3+}$ ions, respectively. The Stokes photoluminescence spectrum upon 378 nm excitation is shown in Fig. 5b. This spectrum is dominated by two strong red lines (654 and 665 nm) attributed to the $^4F_{9/2}$–$^4I_{15/2}$ transition and also contains the weak $^2H_{9/2}$–$^4I_{15/2}$ (406 and 410 nm), $^2H_{11/2}$–$^4I_{15/2}$ (522 nm), and $^4S_{3/2}$–$^4I_{15/2}$ (540 and 550 nm) transitions.

The upconversion spectrum of the $GeO_2$–PbO–$PbF_2$–$YbF_3$–$ErF_3$ glass-ceramics powder demonstrates other intensity distribution. Similar to the Stokes spectrum, the red transition $^4F_{9/2}$–$^4I_{15/2}$ is dominated in the upconversion spectrum, however the green lines ($^2H_{9/2}$–$^4I_{15/2}$ and $^2H_{11/2}$–$^4I_{15/2}$) are much more intensive. In order to understand the upconversion emission mechanism involved in $GeO_2$–PbO–$PbF_2$–$YbF_3$–$ErF_3$ phosphors, the emission intensity dependence on pump power was measured (Fig. 5c). One knows that the

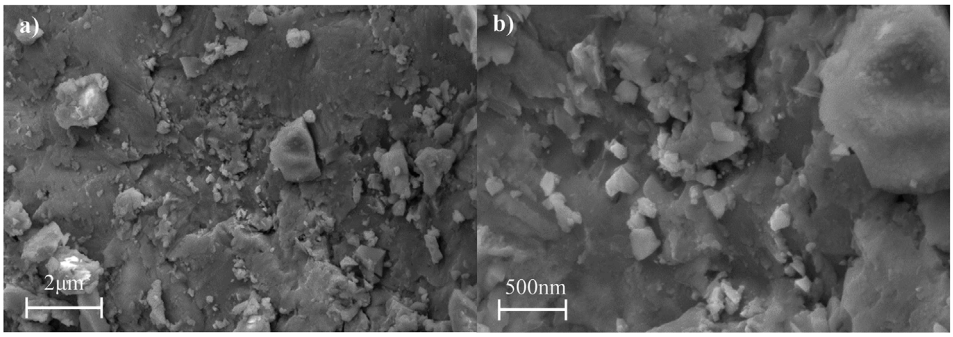


**Fig. 2.** SEM images of $GeO_2$–PbO–$PbF_2$–$YbF_3$–$ErF_3$ glass-ceramics powder.

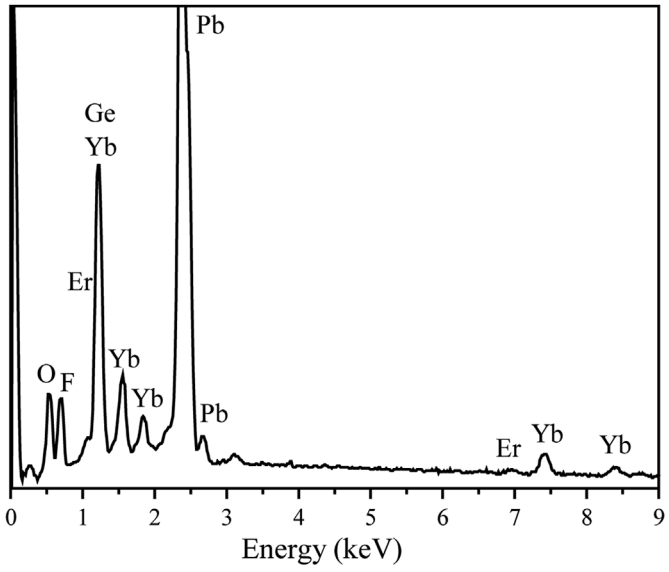


**Fig. 3.** EDX spectrum of $GeO_2$–PbO–$PbF_2$–$YbF_3$–$ErF_3$ glass-ceramics powder.

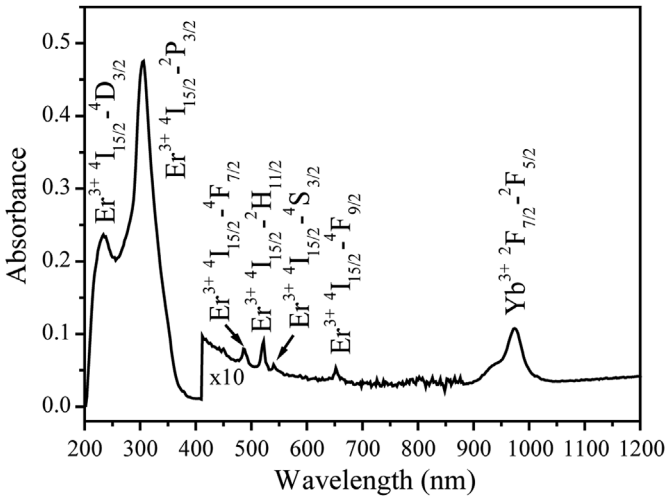


**Fig. 4.** Absorption spectrum of $GeO_2$–PbO–$PbF_2$–$YbF_3$–$ErF_3$ glass-ceramics powder.

upconversion emission intensity ($I_{UC}$) increases proportionally to the pumping power (P) of the excitation source according to: $I_{UC} \sim P^n$, where n is the number of photons needed to pump the population in particular level [27,33]. Therefore, n, the number of photons involved in the upconversion emission can be estimated from the logarithmic plot of the integral emission intensity with the incident laser power. Fig. 5d shows such plot of the integral emission intensity of the green and red emission lines as a function of the pump laser power. The obtained experimental data can be well fitted using linear function with the slopes of 1.77–2.33 on log-log plot. Generally, a straight line with a slope approximately equal to 2 indicates that two photons are involved for the upconversion emission [34]. So, we can draw a conclusion that both green and red emission lines of $GeO_2$–PbO–$PbF_2$–$YbF_3$–$ErF_3$ phosphor arise from a two-photon process [35].

The normalized upconversion spectra of $GeO_2$–PbO–$PbF_2$–$YbF_3$–$ErF_3$ glass-ceramics powder obtained at different temperatures (300, 370, 466 K) are shown in Fig. 6a. As can be seen, the luminescence intensity demonstrates a significant temperature-dependent behavior. The ratiometric luminescence thermal sensing was performed using two approaches: $R_1$ is ratio between $^2H_{11/2}$–$^4I_{15/2}$ (520 nm) and $^4S_{3/2}$–$^4I_{15/2}$ (537 nm) transitions; $R_2$ is ratio between $^2H_{11/2}$–$^4I_{15/2}$ (520 nm) and $^4F_{9/2}$–$^4I_{15/2}$ (652 nm) transitions (Fig. 6b). Usually, the ratiometric temperature sensing is provided by the thermally coupled levels with energy mismatch in the range of 200–2000 $cm^{-1}$ [36]. The energy difference between $^2H_{11/2}$ and $^4S_{3/2}$ levels meets this requirement. In this case, the temperature induced change of FIR is explained by population re-distribution, which is governed by the Boltzmann formula:

$$R_1 = A \cdot \exp\left(-\frac{\Delta E}{kT}\right) \quad (2)$$

where ΔE is the energy gap between the levels, k is the Boltzmann constant, and T is the temperature.

The evolution of $R_1$ with temperature together with fitting curve is presented in Fig. 7a. It should be noted that the calculated energy gap between $^2H_{11/2}$ and $^4S_{3/2}$ levels obtained from the calibration curve ($\Delta E_{calibr} = 817\ cm^{-1}$) perfectly matches with experimental $\Delta E_{spectr} = 820\ cm^{-1}$, which was obtained from the measured upconversion spectrum.

The error δ between $\Delta E_{calibr}$ and $\Delta E_{spectr}$ is given by following equation [37]:

$$\delta = \frac{(\Delta E_{spectr} - \Delta E_{calibr})}{\Delta E_{spectr}} \times 100\% \quad (3)$$

It should be noted that δ was determined to be as small as ~ 0.4% for $^2H_{11/2}$ and $^4S_{3/2}$ levels.

Despite the fact that $^2H_{11/2}$ and $^4F_{9/2}$ levels with energy gap of ~3930 $cm^{-1}$ are non-thermally coupled levels, the thermal dependence of $R_2$ can be fitted by eq. (1) (Fig. 7c). So, $R_2$ value can provide information about the local temperature. Noteworthy, that in this case, ΔE does not have physical meaning as the energy gap between levels.

To date, upconversion materials are widely used as luminescent temperature probes, however it is rarely reported that such phosphors should be utilized as thermometers very carefully. Due to the different excitation power dependences of the upconversion emission transitions, which is used for the thermal sensing, even the ratiometric approach could not provide universal thermal calibration curve for all excitation

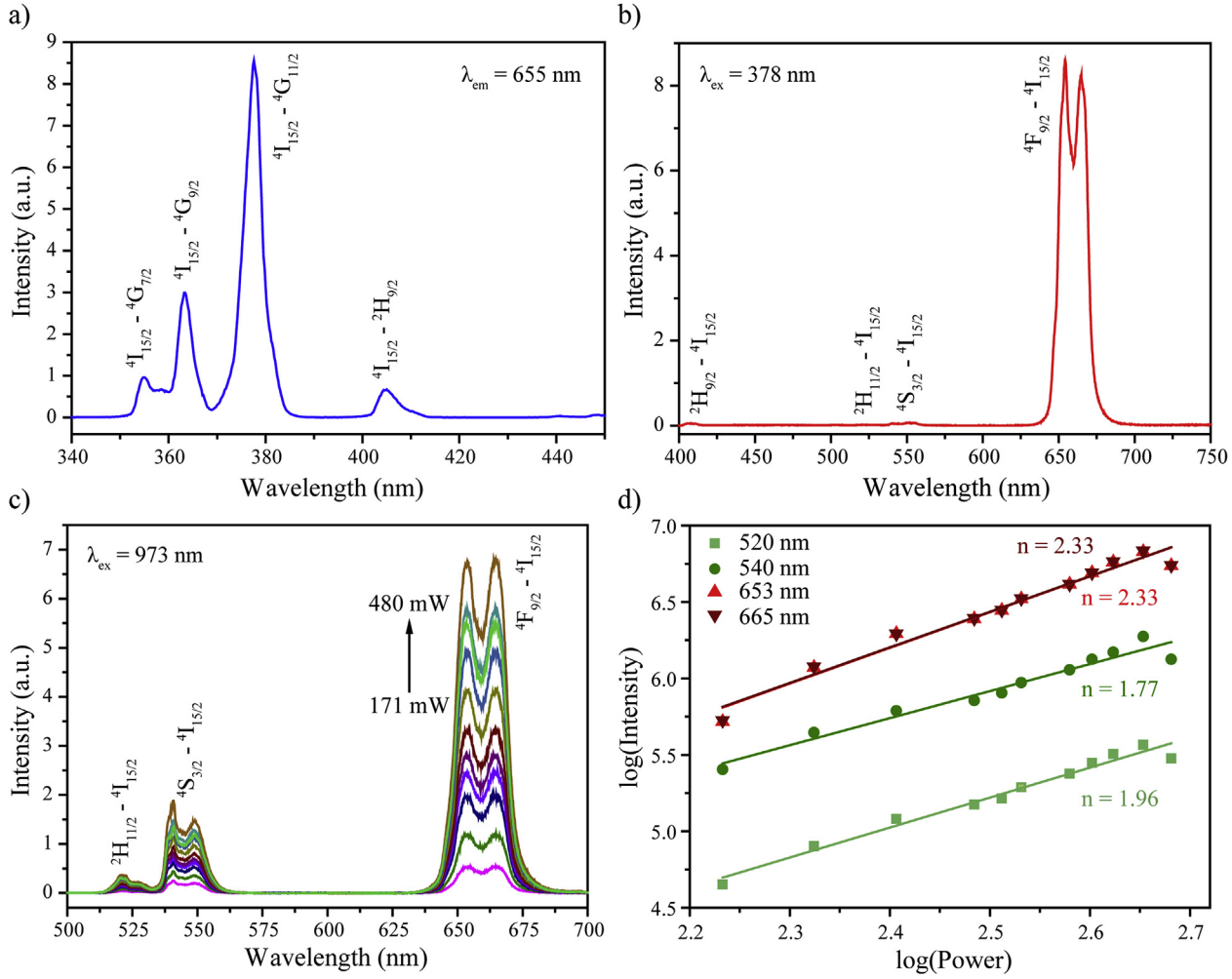


**Fig. 5.** a) Excitation spectrum of $GeO_2$–PbO–$PbF_2$–$YbF_3$–$ErF_3$ glass-ceramics powder; b) Stokes photoluminescence spectrum upon 378 nm excitation; c) upconversion spectrum of $GeO_2$–PbO–$PbF_2$–$YbF_3$–$ErF_3$ glass-ceramics powder upon 973 nm excitation; d) integral emission intensity of the green and red emission lines as a function of the pump laser power. (For interpretation of the references to colour in this figure legend, the reader is referred to the Web version of this article.)

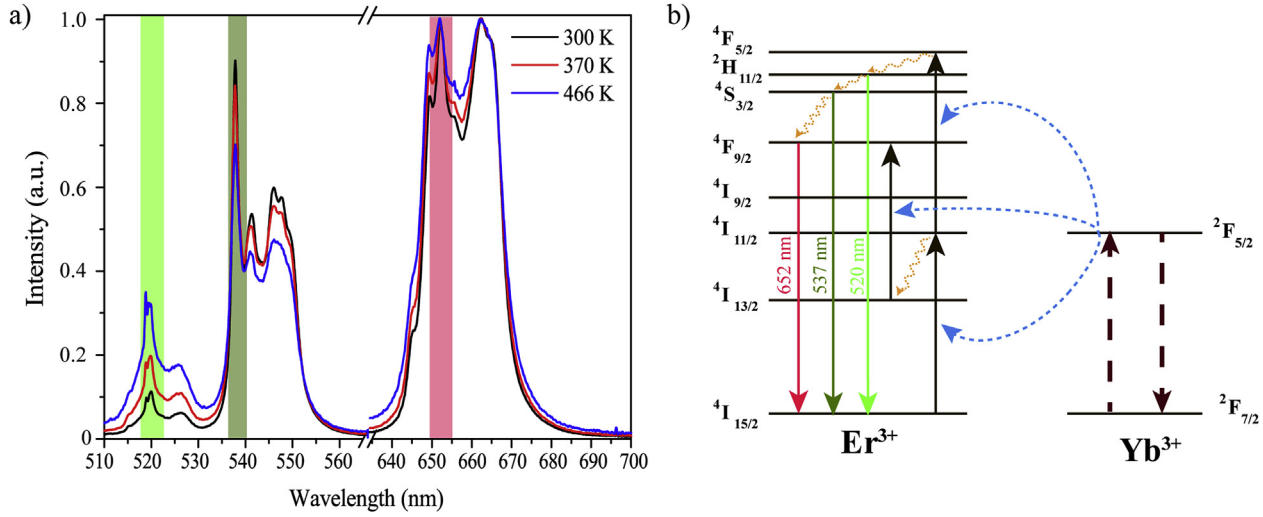


**Fig. 6.** a) Normalized emission spectra of $GeO_2$–PbO–$PbF_2$–$YbF_3$–$ErF_3$ glass-ceramics powder upon 973 nm excitation obtained at different temperatures. The shadowed areas are used for the integral intensity ratio calculations; b) schematic energy level diagram of $Er^{3+}$ and $Yb^{3+}$ ions and mechanisms of upconversion emission.

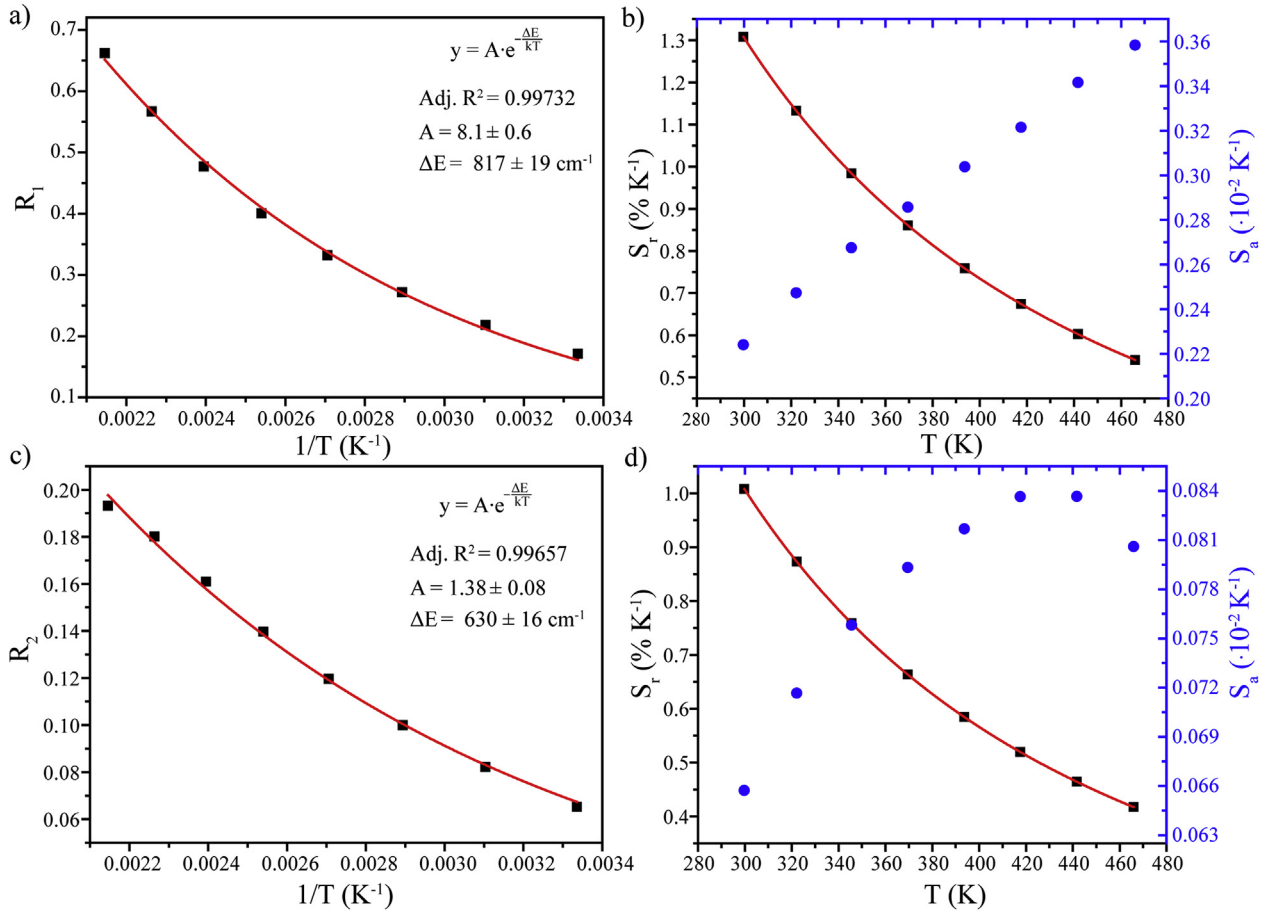


**Fig. 7.** Fluorescence intensity ratio a) $R_1$ and c) $R_2$ as a function of temperature. Variation of absolute ($S_a$) and relative ($S_r$) thermal sensitivity dependent on temperature for b) $R_1$ and d) $R_2$.

powers. Therefore, the individual calibration curve should be obtained for the specific excitation power to perform accurate thermal sensing. Here, laser power of 5 mW was kept during all thermal measurements.

The performance of thermometer is usually characterized by a set of following parameters: the absolute ($S_a$) and relative ($S_r$) thermal sensitivity, the temperature resolution (δT), and the repeatability. The absolute thermal sensitivity defines the absolute FIR change with temperature variation and can be obtained using eq. (3):

$$S_a = \frac{dR}{dT} = R\frac{\Delta E}{kT^2} \tag{4}$$

One can see that $S_a$ depends on absolute FIR value, which can be significantly changed by the manipulating FIR calculation procedure (for instance, change of integration limit for calculation for integral intensity of emission transition). Therefore, the absolute thermal sensitivity is not suitable for the fair comparison among different systems [38].

The relative thermal sensitivity is introduced to compare the thermometers of different nature. It is the normalized change in FIR with temperature variation and is defined as:

$$S_r = \frac{1}{R}\frac{dR}{dT} = \frac{\Delta E}{kT^2} \tag{5}$$

The variation of the $S_r$ and $S_a$ value with temperature from 300 to 466 K for $R_1$ and $R_2$ ratio is illustrated in Fig. 6b and d, respectively. Noteworthy, the observed temperature dependences of $S_r$ and $S_a$ demonstrate opposite behavior: the temperature increase leads to the monotonic decline of $S_r$ and gradual growth of $S_a$. So, the maximum relative thermal sensitivity was obtained at the lowest measuring temperature of 300 K: 1.31% $K^{-1}$ ($R_1$) and 1.1% $K^{-1}$ ($R_2$), whereas the maximum absolute thermal sensitivity was achieved at much higher temperatures: 0.0036 $K^{-1}$@466 K ($R_1$) and 0.0008 $K^{-1}$@441 K ($R_2$). Table 1 presents comparison of temperature range and relative thermal sensitivity for different $Yb^{3+}/Er^{3+}$ doped materials. It should be noted that the $S_r$ values obtained in this work are on a par with the best values for the $Yb^{3+}/Er^{3+}$ systems.

Temperature resolution provides information about accuracy of the thermal sensing using regarded material. As we have shown in our earlier work, the temperature resolution can be calculated in several ways: from calibration curve, from acquisition of several consecutive emission spectra at a fixed temperature and from analysis of thermal relaxation process [52]. Here, the temperature resolution of the thermometer is calculated by the formula:

$$\delta T = \frac{1}{S_r}\frac{\delta R}{R} \tag{6}$$

where δR/R is the relative uncertainty in the determination of the temperature. δR/R value was obtained as dispersion of three repeated measurements, whereas R was the average value of FIR. The calculated temperature resolution is 0.2–0.4 K (300–466 K) for $R_1$ and 0.3–2.0 K (300–466 K) for $R_2$ ratio. It should be noted that despite the temperature resolution is an important parameter, it is quite poorly represented in the recent works on $Yb^{3+}/Er^{3+}$-based optical thermometers. The obtained temperature resolution is comparable with the reported values for $Yb^{3+}/Er^{3+}$ pair. For example, the δT value of 1–5 K is reported for $NaYF_4$:$Yb^{3+}$,$Er^{3+}$/$SiO_2$ core/shell nanocrystals in the temperature range of 290–900 K [53]. The δT value of ~0.3 K is reported for $SrF_2$:$Yb^{3+}$,$Er^{3+}$ nanoparticles in the temperature range of 303–373 K [54].

**Table 1**
Comparison between relative thermal sensitivities of $Yb^{3+}/Er^{3+}$-doped materials calculated by using the ratiometric technique.

| Material | Temperature Range (K) | $S_r$ (% $K^{-1}$) | Reference |
|---|---|---|---|
| $GeO_2$–PbO–$PbF_2$–$YbF_3$–$ErF_3$ ($R_1$) | 300–466 | 1.31@300K | This work |
| $GeO_2$–PbO–$PbF_2$–$YbF_3$–$ErF_3$ ($R_2$) | 300–466 | 1.0@300K | This work |
| $LaF_3$:$Yb^{3+}/Er^{3+}$ | 300–515 | 1.57@386K | [34] |
| $Yb^{3+}/Er^{3+}$ co-doped tellurite glass | 278–473 | 0.53@473K | [39] |
| $Yb^{3+}/Er^{3+}$ co-doped silicate glass | 496–723 | 0.63@296K | [40] |
| $Yb^{3+}/Er^{3+}$ co-doped phosphate glass | 303–753 | 1.22@303K | [41] |
| $NaYF_4$:$Yb^{3+}/Er^{3+}$ glass ceramics | 298–693 | 1.26@298K | [42] |
| β-$NaGdF_4$:$Yb^{3+}/Er^{3+}$ glass ceramics | 303–563 | 0.37@580K | [43] |
| $NaYF_4$:$Yb^{3+}$, $Er^{3+}$ | 175–350 | 1.1@200K | [44] |
| Er,Yb:$Gd_2O_3$/Au NPs | 300 – 1050 | 1.51@303K | [45] |
| $LaGdO_3$:$Yb^{3+}$, $Er^{3+}$ | 283–393 | 1.08@383K | [46] |
| $Gd_2(MoO_4)_3$:$Yb^{3+}$, $Er^{3+}$ | 289.6–510.2 | 1.2@300K | [47] |
| β-$NaYF_4$:$Yb^{3+}$, $Er^{3+}$ | 303–573 | 1.16@303K | [48] |
| $Y_2O_3$:$Yb^{3+}$, $Er^{3+}$ | 125–300 | 1.32@300K | [49] |
| $CaWO_4$:$Yb^{3+}$, $Er^{3+}$, $Sr^{2+}$ | 298–2000 | 1.1@456K | [50] |
| $NaZnPO_4$:$Yb^{3+}$, $Er^{3+}$ | 303–753 | 1.3@303K | [51] |

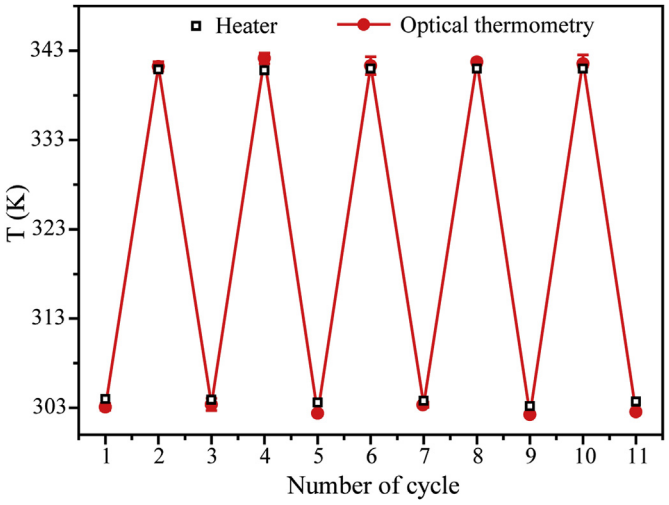


**Fig. 8.** Repeatability of FIR readout during 5 heating-cooling cycles.

Repeatability is an important factor for the assessment of the precision of a thermometric system, referring to the variation in repeating the measurement under identical conditions [55]. Repeatability was tested over cyclic heating-cooling measurements (Fig. 8). During the experiment, the temperature rose to 341 K and dropped to 303 K several times. Black squares indicate the actual temperature of heater, whereas red circles show the temperature calculated by FIR. From Fig. 8, we can clearly see the excellent repeatability of the studied $Yb^{3+}/Er^{3+}$-doped phosphor: the temperatures obtained using optical thermometry are repeated from cycle to cycle and they are in well agreement with the actual heater temperature.

Nowadays, microelectronics occupies a key place in everyday life. Rapid development of technology leads to the miniaturization of electrical elements and as a result to the increase of their number on the printed circuit board. This arises the question of temperature control of the electrical elements during manufacturing and operation. Thermal sensing by the conventional contact and non-contact methods is hampered by the small size of the elements of microelectronics and difficulty of localization.

Here, we demonstrate temperature sensing of the microelectronic component using the ratiometric upconversion technique as a proof of concept. The resistor was placed on the printed circuit board and was connected to the power supply (Fig. 9a). To carry out thermal sensing using luminescence thermometry, a colloidal solution of $GeO_2$–PbO–$PbF_2$–$YbF_3$–$ErF_3$ glass-ceramics powder was prepared and then applied with a thin layer on the top of the resistor. Upconversion luminescence was excited with 973 nm laser radiation (Fig. 9b). The thickness of the phosphor layer was small, so the phosphor had almost no effect on the emissivity of the material. As a control method, the temperature of the resistor was also defined by infrared camera Fluke Ti32 (Fig. 9c). The emissivity of resistor's surface (0.93) was used to calibrate the infrared camera during temperature measurements. The infrared camera and FIR method measured temperature on the same area of the sample. The resistor's temperature was varied by changing electrical current. Fig. 9d shows the resistor temperature obtained from different techniques as a function of the electric power. As can be seen, the temperatures obtained with the luminescence thermometry perfectly match with the data obtained using infrared camera. The spatial resolution was determined by the optical resolution of the collecting system and was about 50 μm (focusing diameter of the laser beam for 4x microscope objective).

## 4. Conclusions

In this work, $Yb^{3+}/Er^{3+}$-codoped $GeO_2$–PbO–$PbF_2$ phosphor was synthesized using traditional melt-quenching technique. XRD pattern demonstrated presence of the amorphous glass and crystalline $PbF_2$ phases. EDX technique confirmed presence of germanium, oxide, lead, fluorine, erbium and ytterbium ions in synthesized sample. Absorption spectrum consisted of the characteristic narrow lines attributed to the 4f intra-configurational electron transitions in $Er^{3+}$ and $Yb^{3+}$ ions. The green and red bands in the upconversion spectrum of $GeO_2$–PbO–$PbF_2$–$YbF_3$–$ErF_3$ are originated from two-photon processes. The upconversion luminescence intensity exhibits significant temperature-dependent behavior. A ratiometric technique involving the $Er^{3+}$ thermally and non-thermally coupled levels ($^2H_{11/2}/^4S_{3/2}$ and $^2H_{11/2}/^4F_{9/2}$, respectively) was used to provide thermal sensing in the 300–466 K temperature range. The performance of suggested optical thermometer was obtained in terms of absolute and relative thermal sensitivities, temperature resolution and repeatability. The maximum $S_r$ and $S_a$ values were found to be 1.31% $K^{-1}$@300 K and 0.0036 $K^{-1}$@466 K for fluorescence intensity ratio between $^2H_{11/2}$ and $^4S_{3/2}$ levels. The minimum temperature uncertainty does not exceed 0.4 and 2 K for $R_1$ and $R_2$ ratio, respectively. Thermal cycling experiments showed good repeatability of the studied thermometer. Temperature measurements of the microelectronic component were carried out using two independent techniques: luminescence and infrared thermometry, which showed similar results. The obtained results demonstrate that $Yb^{3+}/Er^{3+}$-codoped $GeO_2$–PbO–$PbF_2$ phosphor is a perspective candidate for luminescence ratiometric thermometry.

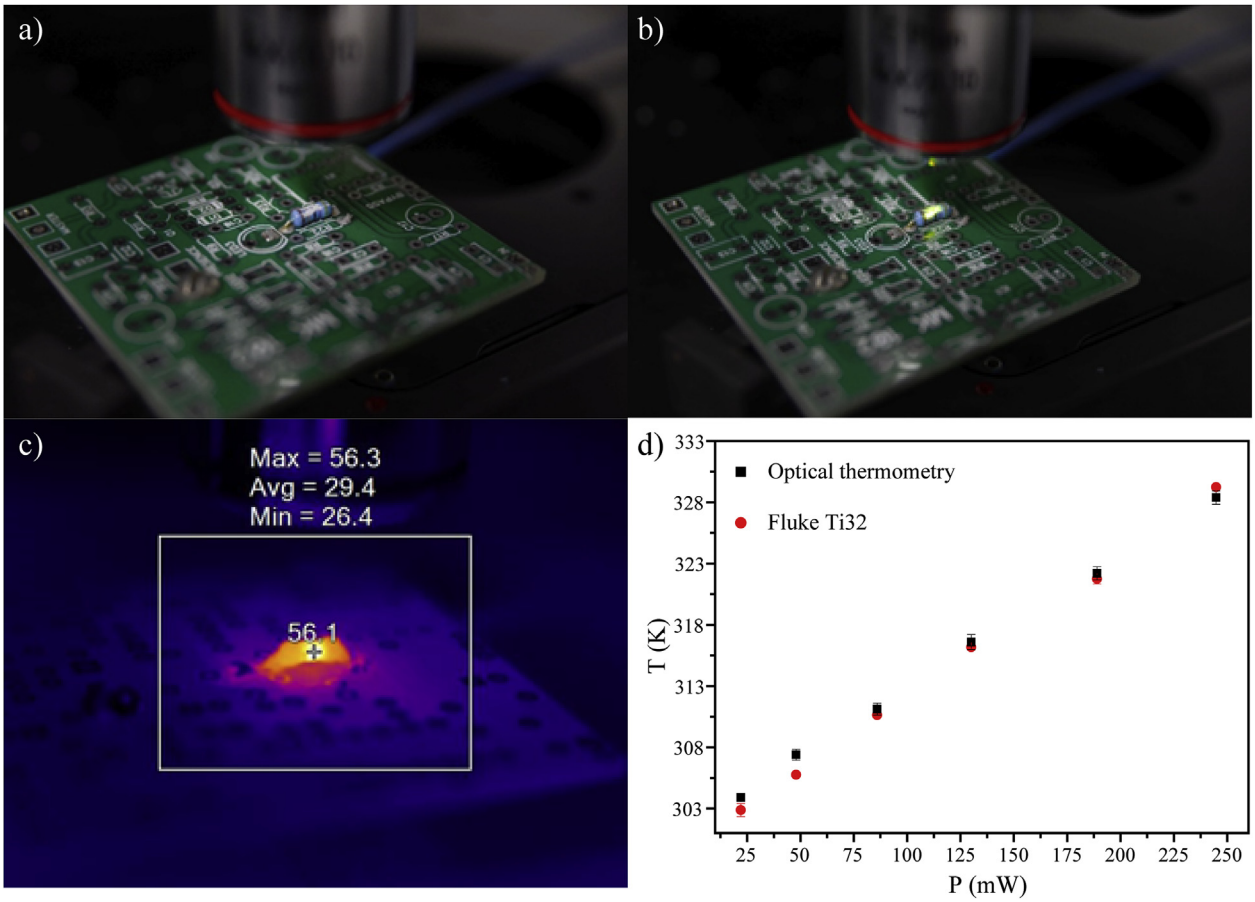


**Fig. 9.** Photos of the resistor with $GeO_2$–PbO–$PbF_2$–$YbF_3$–$ErF_3$ phosphor on printed circuit board at a) day-light and b) upon 973 nm excitation; c) thermal image of the resistor; d) resistor temperature as a function of electric power.

## Acknowledgments

Experimental investigations were carried out in “Center for Optical and Laser materials research“, “Research Centre for X-ray Diffraction Studies“, and “Interdisciplinary Resource Center for Nanotechnology” (St. Petersburg State University).

## References

[1] M. Ding, M. Zhang, C. Lu, Yb3+/Tm3+/Ho3+ tri-doped YPO4 submicroplates: a promising optical thermometer operating in the first biological window, Mater. Lett. 209 (2017) 52–55.
[2] A. Siaï, P. Haro-Gonzalez, K. Horchani-Naifer, M. Férid, La2O3: Tm, Yb, Er up-converting nano-oxides for sub-tissue lifetime thermal sensing, Sensor. Actuator. B Chem. 234 (2016) 541–548.
[3] L.A.O. Nunes, A.S. Souza, L.D. Carlos, O.L. Malta, Neodymium doped fluor-oindogallate glasses as highly-sensitive luminescent non-contact thermometers, Opt. Mater. 63 (2017) 42–45.
[4] X. Wang, Q. Liu, Y. Bu, C.-S. Liu, T. Liu, X. Yan, Optical temperature sensing of rare-earth ion doped phosphors, RSC Adv. 5 (2015) 86219–86236.
[5] A.A. Kalinichev, M.A. Kurochkin, E.V. Golyeva, A.V. Kurochkin, E. Lähderanta, M.D. Mikhailov, et al., Near-infrared emitting YVO4:Nd3+nanoparticles for high sensitive fluorescence thermometry, J. Lumin. 195 (2018) 61–66, https://doi.org/10.1016/j.jlumin.2017.11.024.
[6] X. Wang, O.S. Wolfbeis, R.J. Meier, Luminescent probes and sensors for temperature, Chem. Soc. Rev. 42 (2013) 7834–7869.
[7] Y. Tian, B. Tian, P. Huang, L. Wang, B. Chen, Size-dependent upconversion luminescence and temperature sensing behavior of spherical Gd 2 O 3: Yb 3+/Er 3+ phosphor, RSC Adv. 5 (2015) 14123–14128.
[8] I.E. Kolesnikov, M.A. Kurochkin, A.A. Kalinichev, D.V. Mamonova, E.Y. Kolesnikov, A.V. Kurochkin, et al., Effect of silica coating on luminescence and temperature sensing properties of Nd3+doped nanoparticles, J. Alloy. Comp. 734 (2018) 136–143, https://doi.org/10.1016/j.jallcom.2017.11.048.
[9] W. Xu, Z. Zhang, W. Cao, Excellent optical thermometry based on short-wavelength upconversion emissions in Er 3+/Yb 3+ codoped CaWO 4, Opt. Lett. 37 (2012) 4865–4867.
[10] D. Jaque, F. Vetrone, Luminescence nanothermometry, Nanoscale 4 (2012) 4301, https://doi.org/10.1039/c2nr30764b.
[11] A. Sedlmeier, D.E. Achatz, L.H. Fischer, H.H. Gorris, O.S. Wolfbeis, Photon up-converting nanoparticles for luminescent sensing of temperature, Nanoscale 4 (2012) 7090–7096.
[12] I.E. Kolesnikov, A.A. Kalinichev, M.A. Kurochkin, E.V. Golyeva, E.Y. Kolesnikov, A.V. Kurochkin, et al., $YVO_4$:$Nd^{3+}$ nanophosphors as NIR-to-NIR thermal sensors in wide temperature range, Sci. Rep. 7 (2017), https://doi.org/10.1038/s41598-017-18295-w.
[13] D. Chen, M. Xu, S. Liu, X. Li, Eu2+/Eu3+ dual-emitting glass ceramic for self-calibrated optical thermometry, Sensor. Actuator. B Chem. 246 (2017) 756–760.
[14] Y. Huang, A. Skripka, L. Labrador-Páez, F. Sanz-Rodríguez, P. Haro-González, D. Jaque, et al., Upconverting nanocomposites with combined photothermal and photodynamic effects, Nanoscale 10 (2018) 791–799.
[15] F. Auzel, Upconversion and anti-Stokes processes with f and d ions in solids, Chem. Rev. 104 (2004) 139–174.
[16] H. Dong, L.-D. Sun, C.-H. Yan, Basic understanding of the lanthanide related up-conversion emissions, Nanoscale 5 (2013) 5703–5714.
[17] J.A. Capobianco, F. Vetrone, T. D'alesio, G. Tessari, A. Speghini, M. Bettinelli, Optical spectroscopy of nanocrystalline cubic Y 2 O 3: Er 3+ obtained by combustion synthesis, Phys. Chem. Chem. Phys. 2 (2000) 3203–3207.
[18] J. Zhou, Z. Liu, F. Li, Upconversion nanophosphors for small-animal imaging, Chem. Soc. Rev. 41 (2012) 1323–1349.
[19] E. Hemmer, A. Benayas, F. Légaré, F. Vetrone, Exploiting the biological windows: current perspectives on fluorescent bioprobes emitting above 1000 nm, Nanoscale Horizons 1 (2016) 168–184.
[20] S. Zhou, C. Li, Z. Liu, S. Li, C. Song, Thermal effect on up-conversion in Er3+/Yb3+ co-doped silicate glass, Opt. Mater. 30 (2007) 513–516.
[21] Y. Yang, C. Mi, F. Yu, X. Su, C. Guo, G. Li, et al., Optical thermometry based on the upconversion fluorescence from Yb3+/Er3+ codoped La2O2S phosphor, Ceram. Int. 40 (2014) 9875–9880.
[22] D. Chen, Y. Wang, Y. Yu, P. Huang, Intense ultraviolet upconversion luminescence from Tm 3+/ Yb 3+: β-YF 3 nanocrystals embedded glass ceramic, Appl. Phys. Lett. 91 (2007) 51920.
[23] S. Tanabe, H. Hayashi, T. Hanada, N. Onodera, Fluorescence properties of Er3+ ions in glass ceramics containing LaF3 nanocrystals, Opt. Mater. 19 (2002) 343–349.
[24] P.P. Fedorov, A.A. Luginina, A.I. Popov, Transparent oxyfluoride glass ceramics, J. Fluorine Chem. 172 (2015) 22–50.

[25] J.E. Shelby, E.A. Bolden, Formation and properties of lead fluorogermanate glasses, J. Non-Cryst. Solids 142 (1992) 269–277.
[26] J. Cao, X. Li, Z. Wang, Y. Wei, L. Chen, H. Guo, Optical thermometry based on up-conversion luminescence behavior of self-crystallized K3YF6: Er3+ glass ceramics, Sensor. Actuator. B Chem. 224 (2016) 507–513.
[27] F. Huang, Y. Gao, J. Zhou, J. Xu, Y. Wang, Yb3+/Er3+ co-doped CaMoO4: a promising green upconversion phosphor for optical temperature sensing, J. Alloy. Comp. 639 (2015) 325–329.
[28] Q. Meng, T. Liu, J. Dai, W. Sun, Study on optical temperature sensing properties of YVO4: Er3+, Yb3+ nanocrystals, J. Lumin. 179 (2016) 633–638.
[29] Y. Gao, Y. Hu, D. Zhou, J. Qiu, Effect of heat treatment mechanism on upconversion luminescence in Er3+/Yb3+ co-doped NaYF4 oxyfluoride glass-ceramics, J. Alloy. Comp. 699 (2017) 303–307.
[30] W. Xu, H. Zhao, Y. Li, L. Zheng, Z. Zhang, W. Cao, Optical temperature sensing through the upconversion luminescence from Ho3+/Yb3+ codoped CaWO4, Sensor. Actuator. B Chem. 188 (2013) 1096–1100.
[31] P. Du, L. Luo, J.S. Yu, Upconversion emission, cathodoluminescence and temperature sensing behaviors of Yb3+ ions sensitized NaY (WO4) 2: Er3+ phosphors, Ceram. Int. 42 (2016) 5635–5641.
[32] A.L. Patterson, The Scherrer formula for X-ray particle size determination, Phys. Rev. 56 (1939) 978.
[33] Z. Xia, J. Li, Y. Luo, L. Liao, Comparative investigation of green and red upconversion luminescence in Er3+ doped and Yb3+/Er3+ codoped LaOCl, J. Am. Ceram. Soc. 95 (2012) 3229–3234.
[34] X. Cheng, X. Ma, H. Zhang, Y. Ren, K. Zhu, Optical temperature sensing properties of Yb3+/Er3+ codoped LaF3 upconversion phosphor, Phys. B Condens. Matter 521 (2017) 270–274.
[35] L. Guo, Y.Y. Wang, Y.Y. Wang, J. Zhang, P. Dong, Crystal structure and up-and down-conversion properties of Yb 3+, Ho 3+ codoped BaGdF 5 solid-solution with different morphologies, CrystEngComm 14 (2012) 3131–3141.
[36] V.K. Rai, Temperature sensors and optical sensors, Appl. Phys. B Laser Opt. 88 (2007) 297–303, https://doi.org/10.1007/s00340-007-2717-4.
[37] G. Gao, D. Busko, S. Kauffmann-Weiss, A. Turshatov, I.A. Howard, B.S. Richards, Wide-range non-contact fluorescence intensity ratio thermometer based on Yb 3+/Nd 3+ co-doped La 2 O 3 microcrystals operating from 290 to 1230 K, J. Mater. Chem. C. 6 (2018) 4163–4170.
[38] C.D.S. Brites, P.P. Lima, N.J.O. Silva, A. Millán, V.S. Amaral, F. Palacio, et al., Thermometry at the nanoscale, Nanoscale 4 (2012) 4799–4829, https://doi.org/10.1039/c2nr30663h.
[39] D. Manzani, J.F. da Silveira Petruci, K. Nigoghossian, A.A. Cardoso, S.J.L. Ribeiro, A portable luminescent thermometer based on green up-conversion emission of Er 3+/Yb 3+ co-doped tellurite glass, Sci. Rep. 7 (2017) 41596.
[40] C. Li, B. Dong, S. Li, C. Song, Er3+–Yb3+ co-doped silicate glass for optical temperature sensor, Chem. Phys. Lett. 443 (2007) 426–429.
[41] Y. Chen, X.Y. Liu, G.H. Chen, T. Yang, C.L. Yuan, C.R. Zhou, et al., Up-conversion luminescence and temperature sensing characteristics of Er3+/Yb3+ co-doped phosphate glasses, J. Mater. Sci. Mater. Electron. 28 (2017) 15657–15662.
[42] S. Jiang, P. Zeng, L. Liao, S. Tian, H. Guo, Y. Chen, et al., Optical thermometry based on upconverted luminescence in transparent glass ceramics containing NaYF4: Yb3+/Er3+ nanocrystals, J. Alloy. Comp. 617 (2014) 538–541.
[43] D. Chen, Z. Wan, Y. Zhou, P. Huang, J. Zhong, M. Ding, et al., Bulk glass ceramics containing Yb3+/Er3+: β-NaGdF4 nanocrystals: phase-separation-controlled crystallization, optical spectroscopy and upconverted temperature sensing behavior, J. Alloy. Comp. 638 (2015) 21–28.
[44] L. Marciniak, K. Prorok, A. Bednarkiewicz, Size dependent sensitivity of Yb 3+, Er 3+ up-converting luminescent nano-thermometers, J. Mater. Chem. C. 5 (2017) 7890–7897.
[45] M.L. Debasu, D. Ananias, I. Pastoriza-Santos, L.M. Liz-Marzán, J. Rocha, L.D. Carlos, All-in-one optical heater-thermometer nanoplatform operative from 300 to 2000 K based on Er3+ emission and blackbody radiation, Adv. Mater. 25 (2013) 4868–4874.
[46] A. Siaï, P. Haro-González, K.H. Naifer, M. Férid, Optical temperature sensing of Er 3+/Yb 3+ doped LaGdO 3 based on fluorescence intensity ratio and lifetime thermometry, Opt. Mater. 76 (2018) 34–41.
[47] W. Xu, D. Li, H. Hao, Y. Song, Y. Wang, X. Zhang, Optical thermometry through infrared excited green upconversion in monoclinic phase Gd 2 (MoO 4) 3: Yb 3+/Er 3+ phosphor, Opt. Mater. 78 (2018) 8–14.
[48] M. Ding, Z. Shen, Y. Yuan, W. Bai, C. Lu, Z. Ji, β-NaYF 4: Yb 3+/Er 3+ nanocrystals embedded sol-gel glass ceramics for self-calibrated optical thermometry, Ceram. Int. 44 (12) (15 August 2018) 14884–14890.
[49] V. Lojpur, G. Nikolić, M.D. Dramićanin, Luminescence thermometry below room temperature via up-conversion emission of Y2O3: Yb3+, Er3+ nanophosphors, J. Appl. Phys. 115 (2014) 203106.
[50] X. Wang, Y. Wang, Y. Bu, X. Yan, J. Wang, P. Cai, et al., Influence of doping and excitation powers on optical thermometry in Yb 3+-Er 3+ doped CaWO 4, Sci. Rep. 7 (2017) 43383.
[51] Y. Chen, G.H. Chen, X.Y. Liu, T. Yang, Enhanced up-conversion luminescence and optical thermometry characteristics of Er 3+/Yb 3+ co-doped transparent phosphate glass-ceramics, J. Lumin. 195 (2018) 314–320.
[52] I.E. Kolesnikov, A.A. Kalinichev, M.A. Kurochkin, D.V. Mamonova, E.Y. Kolesnikov, A.V. Kurochkin, et al., New strategy for thermal sensitivity enhancement of Nd 3+-based ratiometric luminescence thermometers, J. Lumin. 192 (2017) 40–46, https://doi.org/10.1016/j.jlumin.2017.06.024.
[53] R.G. Geitenbeek, P.T. Prins, W. Albrecht, A. van Blaaderen, B.M. Weckhuysen, A. Meijerink, NaYF4: Er3+, Yb3+/SiO2 core/shell upconverting nanocrystals for luminescence thermometry up to 900 K, J. Phys. Chem. C 121 (2017) 3503–3510.
[54] S. Balabhadra, M.L. Debasu, C.D.S. Brites, R.A.S. Ferreira, L.D. Carlos, Upconverting nanoparticles working as primary thermometers in different media, J. Phys. Chem. C 121 (2017) 13962–13968.
[55] M. Back, E. Trave, J. Ueda, S. Tanabe, Ratiometric optical thermometer based on dual near-infrared emission in Cr3+-doped bismuth-based gallate host, Chem. Mater. 28 (2016) 8347–8356.